Optics Letters

Measured photoemission from electron wave packets in a strong laser field

Michael Ware,[1,*] Eric Cunningham,[1] Caleb Coburn,[1] and Justin Peatross[1,2]

[1]Department of Physics and Astronomy, Brigham Young University, Provo, Utah 84602, USA
[2]e-mail: peat@byu.edu
*Corresponding author: ware@byu.edu

Received 12 November 2015; revised 20 December 2015; accepted 21 December 2015; posted 5 January 2016 (Doc. ID 253832); published 5 February 2016

We present calibrated measurements of single-photon Thomson scattering from free electrons driven by a laser with intensity 10^{18} W/cm^2. The measurements demonstrate that individual electrons radiate with the strength of point emitters, even when their wave packets spread to the scale of the driving-laser wavelength. The result agrees with predictions of quantum electrodynamics. © 2016 Optical Society of America

OCIS codes: (000.1600) Classical and quantum physics; (270.5580) Quantum electrodynamics; (290.5820) Scattering measurements; (350.5720) Relativity.

http://dx.doi.org/10.1364/OL.41.000689

The founders of quantum mechanics disagreed for a time on the interpretation of the single-particle wave function $\psi(\mathbf{r}, t)$. Schrödinger initially suggested that the quantity $e|\psi(\mathbf{r}, t)|^2$ be interpreted as a classical charge density for the electron [1]. However, this interpretation was soon abandoned in favor of Born's probabilistic interpretation [2], which withstood the subsequent development of quantum electrodynamics (QED). Still, within the semiclassical framework, the Born interpretation does not specify how to couple the electron wave function to the light field. One inevitably must resort to *ad hoc* notions and procedures: Does the emission of a photon constitute a "quantum measurement," perhaps triggering a "wave function collapse?" In the end, QED is needed to address the light-scattering problem consistently, although its formalism lends limited physical intuition.

Within the semiclassical framework, it is natural to associate the quantum probability current with a classical current density $\mathbf{J}$ and use it to generate a (Lorenz-gauge) vector potential [3]

$$\mathbf{A}(\mathbf{r}, t) = \frac{\mu_0}{4\pi} \int \mathrm{d}^3 r' \mathbf{J}(\mathbf{r}', t_r)/R, \tag{1}$$

where $R = |\mathbf{r} - \mathbf{r}'|$ and $t_r = t - R/c$. If $\mathbf{J}$ oscillates with varying phases across its distribution, say in response to a driving laser field, then destructive interference can strongly suppress the scattered radiation $\mathbf{A}$, especially in lateral and reverse directions. Using essentially this approach, Refs. [4,5] found pronounced radiative interference. In particular, dramatic suppression of the scattered radiation results when a single-electron quantum wave packet spreads to the scale of a driving laser wavelength.

These predictions of interference in the radiation field from a single electron wave packet initially seem plausible in the semiclassical view. However, closer inspection shows that such interferences imply near-field work between different portions of the oscillating current distribution [6]. Hence, the possibility of interference in the radiation scattered from a single electron wave packet is on equal footing with the (routinely omitted) possibility of an electron wave packet undergoing Coulomb self-repulsion. In this sense, the expectation of interferences in the radiated light field from a single electron reverts to a Schrödinger-like interpretation, which has undergone occasional tentative revivals [7–9].

We recently demonstrated, using QED theory, that light scattered from a single electron wave packet is independent of the size of that packet [10–12]. Numerical quantum field simulations by Cheng *et al.* support these conclusions [13]. Moreover, from the earliest measurements of Compton scattering, it is apparent that nothing unusual happens when the incident x rays have a wavelength similar in scale to the size of the bound electron wave packets they interact with [14].

Still, it is frequently desirable to compute scattered radiation in a semiclassical framework to avoid the complications of QED. When computing scattered light intensity, classically one expects to square Eq. (1). This squaring of the integral is what gives rise to interference. In a paper that predates QED [15], Gordon skirted the issue by introducing an *ad hoc* step: in essence, he simply moved the square from outside of the integral onto the integrand [6]. While this procedure is inconsistent within the semiclassical viewpoint, it brings the semiclassical result into alignment with the QED result [16,17].

The availability of ultrahigh laser intensities and high-quantum-efficiency photon detectors enables a new direct test of light scattering from free electrons. In particular, these technologies make accessible a regime where *isolated* electrons interact with near-visible wavelengths. The tiny photon-scattering cross section can be compensated for by increasing the intensity. This unprecedented marriage between experimental high-intensity

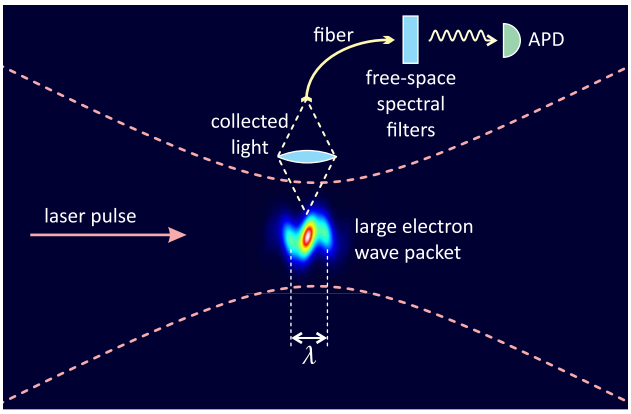

Fig. 1. Single-photon-level light is scattered laterally from large free-electron wave packets in the intense region of a laser focus, collected into a fiber, spectrally filtered, and detected with an APD.

laser physics and quantum optics permits a conceptually clean verification of the QED principle that quantum spreading by free-electron wave packets does not suppress scattering of the incident light. Previously, Thomson scattering has been observed only from dense ensembles of electrons embedded in a plasma and in close proximity compared to the driving wavelength.

In this Letter, we report photon-scattering experiments involving sparse free electrons associated with pressures as low as around 10^{-6} Torr, interacting with an intense laser field. A schematic diagram of the experiment is depicted in Fig. 1. An ultrashort laser pulse is focused in dilute helium to liberate electrons. A later pulse accelerates electron wave packets after they have had time to expand in size. The single-photon-level light scattered from the individual electron wave packets is observed in a direction perpendicular to the propagation, where Eq. (1) would predict very strong suppression due to interference. This represents the successful execution of an experiment proposed in 2008 [10].

The experimental setup is described in detail in Ref. [18]. In short, a 20 mJ, 800 nm laser pulse is focused to a spot size of $w_0 = 5$ μm. The duration of the pulse is 38 fs, as measured using GRENOUILLE Model 8-9-USB. These pulse parameters suggest that the peak laser intensity in our setup is 1.0×10^{18} W/cm^2. We confirmed this intensity using a removable ion time-of flight apparatus which measured the eighth charge state of neon, which is produced at approximately 2×10^{17} W/cm^2 [19]. We still detected this charge state when attenuating the beam by up to a factor of 5.

Our simulations [18] show that 10^{18} W/cm^2 is an ideal intensity range for this experiment. At this intensity, liberated electrons drift in the direction of laser propagation at a significant fraction of the speed of light, so that scattered light is redshifted when viewed from the side. This redshift allows discrimination of the signal photons from background laser light using spectral filters. At our intensity, the redshifted signal peaks at around 900 nm [18], so we use spectral filters to restrict the detected light to the 875–925 nm range. Intensities significantly higher than 10^{18} W/cm^2 would cause the scattered light to be redshifted beyond the spectral range of the avalanche photodiode (APD) and also cause the scattered light to be spatially skewed in the direction of laser propagation.

Photons scattered from the focus, in a direction perpendicular to both the laser propagation and the direction of laser polarization, are collected using a one-to-one imaging lens pair ($f = 50$ mm, 25 mm diameter). The collected light is coupled into a 105 μm optical fiber with a gold coating, which guides the light out of the experimental chamber. The light then passes through a free-space optical bench with a bandpass filter (Thorlabs FB900-40) and two longpass filters (Thorlabs FEL0850), then back into a fiber, and finally into a fiber-coupled APD (Perkin Elmer SPCM-HQR-12-FC). We measured the efficiency of this collection system by coupling light from a 900 nm laser diode into a 62 μm fiber, placing the output end of the fiber at the location of the laser focus, and measuring the fraction of the output light that arrives at various stages of the collection system. The collection lenses couple at least 80% of the light into the fiber, and the free-space spectral filtering system transmits 30% of the in-band light into the final fiber while blocking 800 nm light with an optical density of 17. The APD detector registers 20% of the photons that reach it with 1 ns timing resolution. The overall measured efficiency of this system is such that 5% of the in-band photons emitted into the 0.2-steradian solid angle subtended by the collection lens are registered by the APD.

The 0.9-m-diameter chamber allows prompt photons scattered directly from the laser focus to be distinguished from background photons scattered from the chamber walls. Figure 2 plots the measured counts as a function of delay with the collection system aligned. The upper curve (blue) shows the background count rate in the absence of spectral filtering when the chamber is evacuated to 10^{-8} Torr. Since the laser pulse is not spectrally blocked for this curve, a large number of photons reach the detector, including photons from weak laser prepulses. APD dead time allows at most one detection event per laser shot, so a series of calibrated neutral-density filters was used to trace out the different portions of this curve. The time origin for Fig. 2 is set where light scattered directly from an obstruction temporarily placed in the focus readily

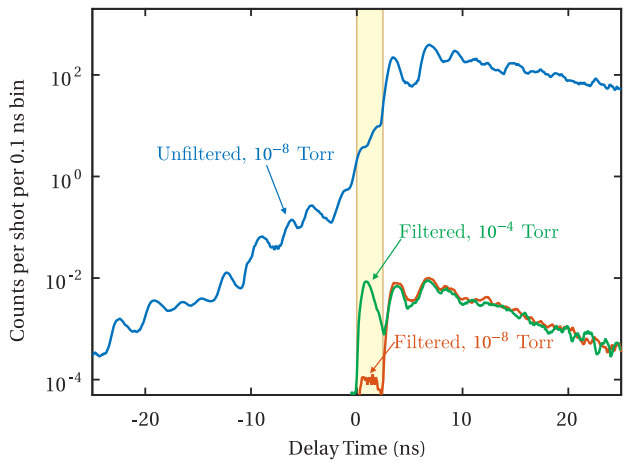

Fig. 2. Time-resolved background level with no spectral filtering (top blue curve) compared to the background level with the spectral filtering in place (bottom red curve). When 10^{-4} Torr of helium is introduced with the filtering in place, a distinct prompt signal becomes distinguishable above the background (green middle curve). The filtered background shows traces of the prompt signal, most likely due to the electrons donated from residual atmospheric gases in the focus.

causes the detector to fire. The shaded 2.5 ns time window represents the time it takes for light from the focus to travel to the chamber wall and back to the collection system. The high background level plotted in the top curve includes the laser wavelength, and highlights the importance of spectral filtering to detect only photons that are relativistically redshifted.

The lowest curve (red) in Fig. 2 represents the background signal with spectral filtering in place. Importantly, photons arising from the laser prepulses are essentially eliminated. Finally, the middle (green) line shows the spectrally filtered signal when 10^{-4} Torr of helium is introduced into the interaction chamber. Note the clearly distinguishable signal that appears during the prompt time window. This prompt redshifted signal is the signature of light scattered from the ionized free electrons that drift forward relativistically in the most intense part of the focus. In summary, a combination of temporal, spectral, and spatial filtering is necessary to extract the genuine signal of light scattering from free electrons.

To make a measurement, we continuously leak helium into the chamber with vacuum pumps running, after achieving a background pressure of 10^{-8} Torr. We measured the redshifted scattered photons as a function of several parameters: helium pressure, laser polarization orientation, prepulse delay, and laser intensity. The photon signal varied linearly with helium pressure, which is an important check against noise from stray light from chamber walls or from collisions between electrons with ions produced in the focus (which ought to exhibit a quadratic pressure dependence). The scattered photon signal vanishes when the linear laser polarization is rotated to aim toward the collection lens, as expected.

Figure 3 plots the count rate as a function of the helium pressure. We expect our signal level to scale directly with pressure (i.e., the number of atoms in the focus), as indicated by the dashed line. Prompt signals are also observed at lower pressures (below 10^{-6} Torr), but at these lower densities, a significant fraction of the relatively few free electrons present are donated from background contaminants (nitrogen, oxygen, water vapor, etc.). In the intense regions of the focus, both electrons in each helium atom are easily ionized at intensities 2 orders of magnitude below the peak intensity. A photon signal could be easily discerned at helium pressures as low as 10^{-6} Torr. This amounts to only one helium atom per 30 cubic microns.

To test for dependence on the electron wave packet size, a relatively weak copropagating laser prepulse was used to

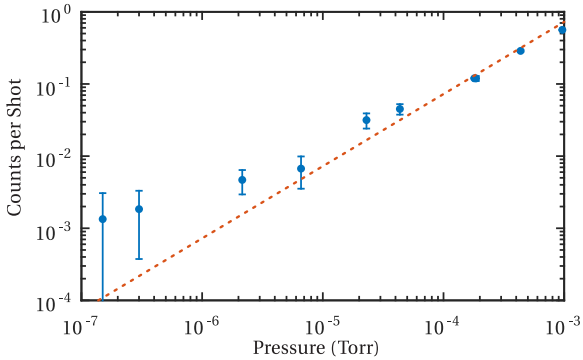

Fig. 3. Count rate as a function of pressure. Error bars show the standard deviation of the count rate measured in one-minute intervals. The dashed line indicates the linear variation of the count rate that is expected due to changes in the number of atoms in the focus.

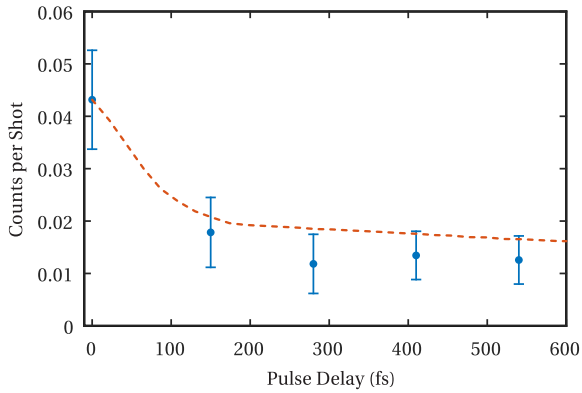

Fig. 4. Photon counts as a function of prepulse delay. The laser pulse has 20 mJ and the prepulse 2 mJ. Ambient pressure is 10^{-5} Torr, and the error bars show the standard deviation of the count rate measured in one-minute intervals. The dashed line shows a computational model that calculates the average emission from pairs of point electrons released at random positions and accelerated by a prepulse and a main pulse with varying delays.

preionize the helium. This allows the electron pairs from individual helium atoms time to separate and gives the electron wave packets time to spread to a scale larger than the laser wavelength before the primary laser pulse arrives. Figure 4 shows the photon count rate as a function of prepulse delay. The prepulse, which carried 10% of the energy of the main pulse, was formed using a thin pellicle in front of a retroreflecting mirror in the laser system. The prepulse delay was directly observed by autocorrelation in a thin KTP crystal (with uncertainty below 5 fs).

One would expect the prepulse to cause a factor of 2 drop in signal, because it allows time for the two ionized electrons from each helium atom to drift apart sufficiently so that they no longer coherently enhance each other's radiation. Commensurately, individual electron wave packets should undergo a similar spreading, owing to ionization over several laser cycles in the presence of strong ponderomotive gradients [5]. The wave packets are expected to spread to the scale of a laser wavelength and larger in approximately a hundred femtoseconds. Following the approach of Eq. (1), such large wave packets would suppress the scattered radiation by 2 or more orders of magnitude owing to interference [10]. However, the drop in signal in Fig. 4 merely exhibits the expected factor of 2 for decohering electron pairs. The fact that the rate of scattered light does not plummet with prepulse delay is direct evidence that scattered radiation is independent of wave packet size.

At the two ionization intensities for helium, the electron drift velocities associated with breaking away from the parent ion are $v = 0.007 \sin\varphi$ μm/fs and $v = 0.019 \sin\varphi$μm/fs, respectively, where φ represents the breakaway phase (with $\varphi = 0$ corresponding to the peak of the field). Presumably, different pieces of the same wave packet have different breakaway phases φ as the wave function bleeds away during several laser oscillations. A reasonable range for the breakaway phase in the vicinity of a particular oscillation peak is $\varphi = \pm\pi/6$. This phase range translates into a range of drift velocity of $v = \pm 0.004$ μm/fs and $v = \pm 0.010$ μm/fs, in the direction of laser polarization. Given these relatively modest velocities, the trajectories of electron pairs from doubly ionized helium

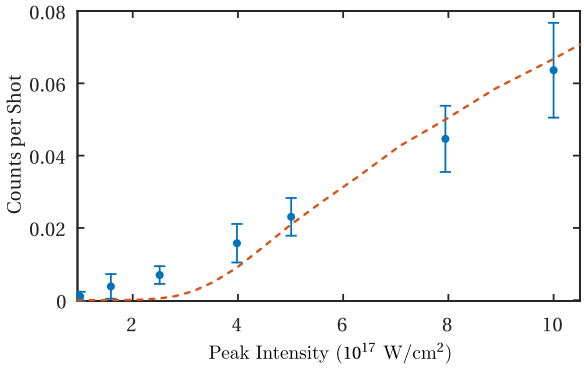

Fig. 5. Photon counts as a function of laser intensity, varied by attenuation of laser energy. Error bars show the standard deviation of the count rate measured in one-minute intervals. The dashed line plots the calculated prediction for radiation from Ref. [18]. Ambient pressure is 3×10^{-5} Torr.

tend to remain correlated in the laser field over several tens of femtoseconds. However, they would typically separate by more than a wavelength if the timescale exceeds a hundred femtoseconds. This is the same time scale that allows an individual wave packet to spread to the size of a laser wavelength. Natural quantum spreading for a free wave packet initially the size of a helium atom spreads (via the uncertainty principle) at a rate of ± 0.003 μm/fs, which is remarkably on par with the spreading due to the range of breakaway phases mentioned above.

In addition to the estimations above, we also compared our measured results with a computational model, plotted as the dashed line in Fig. 4. In this model, two classical point electrons are released sequentially from random locations in the prepulse focus when the local intensity reaches the first and second ionization thresholds for helium. Using many such trajectories, we calculate the average electron separation as a function of delay. We then calculate the average combined emission from these pairs of electrons as they are accelerated by the main laser pulses to find the expected emission level as a function of pulse delay. This model neglects any effects due to interference between the prepulse and the main pulse if they were to temporally overlap at very small delays. As expected, the model shows that with no delay between the pulses, the electrons radiate coherently because they do not have time to spatially separate. As the delay increases such that the electrons separate by about a wavelength or more (on average), the radiation from the two electrons becomes incoherent and the overall signal drops by the expected factor of 2. For comparison purposes, the model is normalized so that the emission level at zero delay matches the experimentally measured value.

Figure 5 plots the emission level as a function of laser intensity when no prepulse is present. The measured values are plotted as points with error bars showing the standard deviation in one-minute counting intervals. The dashed line shows the predicted photon counts from the final simulation of in Ref. [18], which is based on the same parameters as in the experiment. The simulation treats electrons as classical point charges for purposes of computing the strength of light scattering. More details on the simulation techniques may be found in Ref. [18].

The model in Fig. 5 predicts a significant increase in counts as the intensity increases above about 2.5×10^{17} W/cm^2. This threshold effect is due to redshifting. As the laser intensity increases, electrons drift forward at higher velocities and the peak emission spectrum shifts to longer wavelengths as viewed from the side. At intensities around 2.5×10^{17} W/cm^2, the redshifted signal begins to overlap with our detection bandwidth in the 875–925 nm range. The measured data show a more gradual change in slope than the model, due in part to a gradual transition from blocking to transmission at the 875 nm edge of the filter. All parameters such as laser intensity, focus size, and bandpass transmittance were set to match measured experimental parameters, with no free parameters. The differences between the experimental results and the theoretical predictions are likely impacted by several unknowns relating to the exact temporal and spatial distribution of the fields in the focus as compared to our idealized analytic model.

The important result here is that the measured count rate is close to that predicted from classical point emitters. This would not be the case if the radiation were suppressed by a spreading of the electron wave functions. This experiment thus distinguishes between the two pictures of photon emission discussed in this Letter. According to Eq. (1), light scattering from large wave packets should be suppressed by orders of magnitude. On the other hand, QED dictates that scattering occurs with the same strength as point emitters, regardless of the size of the wave packet.

Funding. National Science Foundation (NSF) (PHY-0970065).

Acknowledgment. We appreciate and thank the following students who participated in this research: Matthew Ashby, James Fletcher, Colin Mann, and Kamal Pangeni.

REFERENCES

1. E. Schrödinger, Phys. Rev. **28**, 1049 (1926).
2. M. Born, Z. Phys. **37**, 863 (1926).
3. D. J. Griffiths, *Introduction to Electrodynamics*, 4th ed. (Pearson, 2013).
4. P. Krekora, R. E. Wagner, Q. Su, and R. Grobe, Laser Phys. **12**, 455 (2002).
5. E. A. Chowdhury, I. Ghebregziabiher, and B. C. Walker, J. Phys. B **38**, 517 (2005).
6. J. Peatross, J. P. Corson, and G. Tarbox, Am. J. Phys. **81**, 351 (2013).
7. A. Barut, Found. Phys. Lett. **1**, 47 (1988).
8. E. T. Jaynes, in *The Electron*, D. Hestenes and A. Weingartshofer, eds. (Kluwer, 1991), pp. 1–20.
9. L. Johansson, *Interpreting Quantum Mechanics* (Ashgate, 2007).
10. J. Peatross, C. Müller, K. Z. Hatsagortsyan, and C. H. Keitel, Phys. Rev. Lett. **100**, 15360 (2008).
11. J. P. Corson, J. Peatross, C. Müller, and K. Z. Hatsagortsyan, Phys. Rev. A **84**, 053831 (2011).
12. J. P. Corson and J. Peatross, Phys. Rev. A **84**, 053832 (2011).
13. T. Cheng, C. C. Gerry, Q. Su, and R. Grobe, Europhys. Lett. **88**, 54001 (2009).
14. C. Barrett, Phys. Rev. **32**, 22 (1928).
15. W. Gordon, Z. Phys. **40**, 117 (1926).
16. J. D. Bjorken and S. D. Drell, *Relativistic Quantum Mechanics* (McGraw-Hill, 1964).
17. J. Lacki, H. Ruegg, and V. L. Telegdi, Stud. Hist. Philos. Modern Phys. **30**, 457 (1999).
18. G. Tarbox, M. Ware, and J. Peatross, J. Opt. Soc. Am. A **32**, 743 (2015).
19. S. Augst, D. Strickland, D. D. Meyerhofer, S. L. Chin, and J. H. Eberly, Phys. Rev. Lett. **63**, 2212 (1989).